Designed polymers for laser-based microthrusters – correlation of thrust with material, plasma, and shockwave properties

L. Urech[a], M. Hauer[a], T. Lippert*[a], C. R. Phipps[b], E. Schmid[a], A. Wokaun[a], I Wysong[c]
[a]Paul Scherrer Institut, Villigen, Switzerland
[b]Photonic Associates, USA
[c]European Office of Aerospace Research & Development, UK

ABSTRACT

The micro laser plasma thruster (μLPT) is a micropropulsion device, designed for the steering and propelling of small satellites (10 to 100 kg). A diode laser is focused on a two-layer polymer tape, where it forms a plasma. The thrust produced by this plasma is used to control the satellite motion. Three different polymers (GAP, PVN and PVC) doped with carbon and/or IR-dye were investigated for their performance as fuel polymer. The different dopants for GAP seem to have only little influence in the ablation properties. The most pronounced differences are observed in the fragment ejection detected in the shadowgraphy measurements and the crater appearance. For all carbon doped polymers, the ablation spots have a similar rough morphology. The shadowgraphy measurements of PVN reveal, that the shockwave and particle plume propagates faster as in the case of the other polymers. The particle plumes showed a very different expansion behavior for all polymers, whereas the plasma temperature and electron density measurements showed no significant difference. Only PVC displayed a slower almost liner drop of the plasma temperature over time. The thrust measurements showed the best results for GAP.

1. INTRODUCTION

The micro-Laser Plasma Thruster (μLPT) offers a new option in the field of micro-propulsion for both civilian and military space missions. It meets the requirements of low mass, volume and power consumption, which are critical for these micro satellite platforms.
In order to obtain bidirectional thrust on three axes, six single-axis thrust units are needed. For a 25-kg satellite, a low weight of these propulsion devices (less than one kg) is the most important criteria. Other requirements are at least 75 μN thrust and 300 N-s lifetime impulse [1, 2].

The μLPT will be the first macroscopic application of laser ablation to space propulsion. It takes advantage of the predictable physics in laser–material interaction, where a pulsed laser interacts with a polymer, and thereby forms a plasma. Due to the confining forces involved in the plasma formation, no nozzle is required to direct the jet. The functional principle of a μLPT is shown in Fig 1 [1].

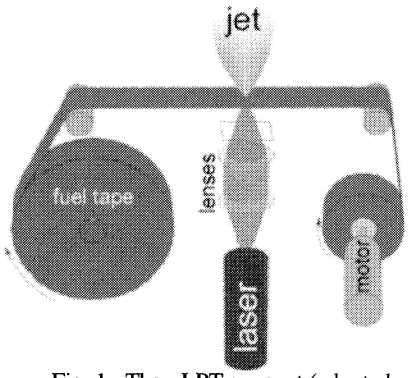

Fig. 1. The μLPT concept (adapted from [1].

The μLPT is driven by small powerful diode lasers, which emit in the near IR (930-980 nm) with an available power of around 1 to 5 W and a pulse length from 100 μs to the millisecond range [3]. This pulse duration and wavelength require the utilization of materials for the fuel layer with low thermal conductivity, i.e. polymers [3, 4]. The laser beam is focused on a polymer tape consisting of a transparent supporting layer, through which the light passes without perforating it, and an absorbing fuel layer, where the micro-jet is produced by the laser-material interaction. The power density on the target is optically variable, allowing to adjust the operating parameters instantly to match the mission requirements. The easy fuel supply through the tape design and the effective usage of the fuel, which is achieved by focusing the laser to a focal spot of about 140 μm are a big advantage of this setup.

* thomas.lippert@psi.ch; phone 0041 56 3104076; fax 0041 56 3102688

High-Power Laser Ablation V, edited by Claude R. Phipps, Proceedings of SPIE
Vol. 5448 (SPIE, Bellingham, WA, 2004) · 0277-786X/04/$15 · doi: 10.1117/12.544771

Another benefit of this setup is the protection of the optics by the support layer from contamination. It builds a physical barrier between the plasma and the lenses. Requirements for the support layer are transparency for near IR light, flexibility and resistivity to solvent and moisture, toughness, low outgassing and high optical damage resistance. Materials that have been tested for the support layer are cellulose acetate, poly(ethylene terephthalate), fluorinated ethylene-propylene and Kapton™. As the required properties tend to be mutually exclusive, different substrates were used, depending on the fuel polymer. For general use, cellulose acetate showed the best overall performance, but was not resistant to solvents used in the preparation of the GAP films. Kapton™, which was used for the GAP films has excellent toughness and outgassing properties, but a lower optical damage resistance compared to cellulose acetate [1, 5].

2. EXPERIMENTAL

In order to understand the influence of the specific properties of the used fuel layer polymers, three different "high"- and "low"-energetic polymers (see table 1) were used: Glycidyl acide polymer (GAP, obtained from Nitrochemie, Wimmis) and Poly(vinyl nitrate) (PVN, synthesized according to [6]), and Poly(vinyl chloride) (PVC, obtained from Aldrich) as a low-energetic reference polymer that showed the best properties among commercial polymers [7] (chemical structure shown in Fig. 2). The polymers were doped with carbon (nanoparticles) and an IR-dye in the case of GAP, in order to reach absorption in the near IR (at a wavelength of 1064 nm). The main difference between the IR-dye and the carbon is, that the dye should be distributed homogenously within the polymer on a molecular level, whereas the carbon remains as particles with a minimum diameter of 15 nm or as agglomerates with particle sizes of up to 20 μm in the polymer [8].

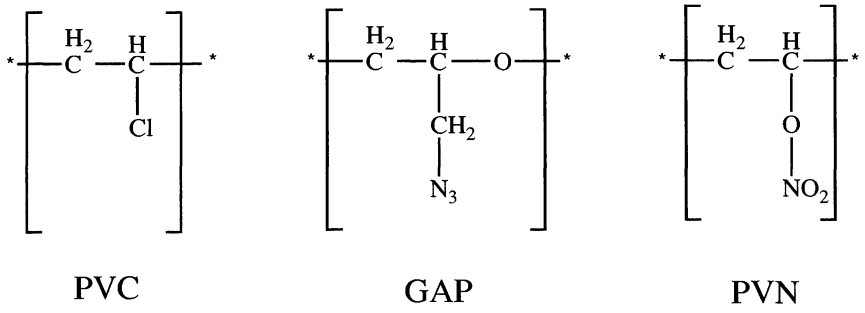

Fig.2. The chemical structure of the studied polymers

The dopant concentration was adjusted to obtain an OD of ≈ 4 at 1064 nm for a 100 μm thick film for all experiments. This absorbance was chosen to achieve an absorption of the laser photons within the complete polymer layer. Previous experiments had shown, that strong absorption at the support-fuel-layer interface, will result in the creation of a "flyer" consisting of the polymer above the absorption zone. A flyer would of course result in a reduction of the energy that could be gained by the decomposition of the energetic polymers, or the thrust gained from the plasma. If the laser pulse is homogeneously absorbed in the complete layer, a uniform ablation takes place and more material can be decomposed.
Four different types of carbons were tested as dopants to induce absorption in the near IR: basic, acidic, conductive carbon, and also carbon in the form of nanopearls with a nominal size of 15 nm. For GAP and PVC carbon nanopearls were used, while for PVN basic carbon was applied, as the nanopearls agglomerated to fast, and a stable carbon suspension could not be obtained in acetone. For all polymers, the dopant was dispersed in the same solvent as the polymer (see table 1), by shaking in the case of IR-dye, and by mixing with an high-speed stirrer (Ultra-Turrax® T25 basic from IKA®) in the case of the carbon solutions. The dopant suspensions were then mixed with to the polymer solution prior to preparing the polymer layer by solvent casting with a draw blade. The polymers will be revered to in this paper with the abbreviation of the polymer and by indicating the dopant by "+ C" for carbon and "+ IR" for IR-dye.

Table 1.: Solvents used for solvent casting GAP, PVN and PVC and the decomposition properties of the three polymers.

Polymer	Solvent	Decomposition Temperature [°C]	Decomposition* Enthalpy [J/g]
GAP	Ethyl acetate	249	-2053
PVN	Acetone	204	-3829
PVC	Cyclohexanone	241,288,383	-418

*measured by DSC, using carbon doped samples of the polymer.

For all experiments (except thrust measurements) the 1st harmonic (λ =1064 nm) of a Nd:YAG laser (Brilliant BW Nd:YAG, Quantel, τ= 6 ns) with a Super-Gaussian beam profile that contains some hotspots was applied. The ns-shadowgraphy, plasma emission spectroscopy, and ablation experiments were performed at room temperature under ambient conditions.

The ablation rates were studied for all polymers as a function of the laser fluence. The depth of the ablation craters was then measured with a surface profilometer (Sloan Dektak 8000). The ablation parameters, α_{eff} (effective absorption coefficient) and F_{th} (threshold fluence) were calculated according to equation 1[9 - 11]:

$$d(F) = \frac{1}{\alpha_{eff}} \ln\left(\frac{F}{F_{Th}}\right) \quad (1)$$

The plasma threshold fluence (F_{plasma}) was determined by visually detecting the onset of plasma formation with increasing laser fluence.

The ns-shadowgraphy measurements were performed in a pump-probe setup (shown in Fig. 2). The pump laser (λ = 1064nm) was focused on a 400 μm spot on the target film. The ejected fragments and shockwave were illuminated by the fluorescence of a rhodamine 950 (from Exiton)-ethanol solution, which was excited by a XeCl excimer laser (λ = 308 nm, Compex 205 from Lambda Physics, τ = 30 ns). The resulting images were recorded by a digital camera (C-MOS)which was orientated parallel to the sample surface.
The delay time between probe laser (excimer) and the pump laser (Nd:YAG) was varied in the range of –100 to 3000 ns with a delay generator (DG 535 from SRS), allowing time resolved imaging of the shockwave propagation and particle ejection.

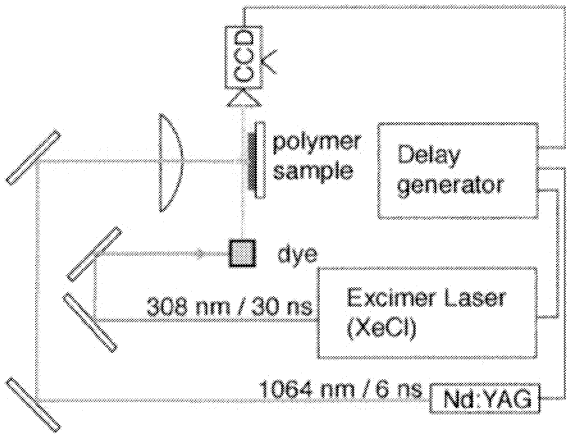

Fig. 3. Schematic setup of the ns-shadowgraphy experiment.

The plasma emission spectroscopy experiments were performed above the fluence where plasma can be observed (F_{plasma}) for all polymers. The plasma emission was collected and focused on the end of an optical fiber by a two lens setup. The light was then dispersed in a spectrometer (Spectra Pro 500 from Acton) and recorded by a gated ICCD (ICCD-1024-MLDG-E/1 with a PG-200 Pulse generator (PG-200), both from Princeton Instruments).
Generally, a 1800 g/mm grating with an optimal working range from 330 to 850 nm was used in all experiments. Overview spectra from 200 nm to 700 nm were acquired for all polymers at different fluences with a 1 μs delay to the incident laser beam. Detailed spectra of the CN Violet system at 389 nm and of the Hydrogen-Balmer-α at 656 nm were recorded from 50 ns until the signal to noise ratio reached a value of 2 (roughly after 15 μs).

2.1. Simulation of the diatomic plasma emission

The relative complex structure of the emission spectra of diatomic molecules such as CN is due to the combination of the electronic transition from the different rotational and vibrational states.

The LIFBASE [11] program was used to estimate the "temperatures" in the plasma. LIFBASE calculates the spectra of diatomic molecules by summing the intensity of all rotational and vibrational levels and convoluting the result with the instrumental line shape of the optical system. The intensities are obtained using equation 2:

$$I_{v''J''}^{v'J'} = KA_{v''J''}^{v'J'}N_{v'J'} \qquad (2)$$

K is an experimental constant taking the sensitivity of the optical system into account, while $N_{v'J'}$ is the population in the excited state. A Boltzmann distribution can be used to determine $N_{v'J'}$, when a thermal distribution of the states of the molecules is assumed.

The Einstein coefficient $A_{v''J''}^{v'J'}$ was calculated according to equation 3:

$$A_{v''J''}^{v'J'} = \frac{g_e'}{g_e''}\frac{64\pi}{3h}\frac{S_{J''}^{J'}}{2J'+1}p_{v''J''}^{v'J'}(\upsilon_{v''J''}^{v'J'})^3 \qquad (3)$$

were g_e is the electric degeneracy which takes the state spin multiplicity into account. S is the line strength or Honl-London factor, which was used following the analytical expression by Kovacs [12] and Earls [13]. The transition probability p was calculated previously and included in the database of the program, while υ is the transition frequency.

The "plasma" temperatures were estimated by calculating the ro-vibrational spectra of the CN-violet system ($B^2\Sigma \rightarrow X^2\Sigma^+$) for different temperatures. A calculated spectra for the different vibration levels is shown in Fig. 4.

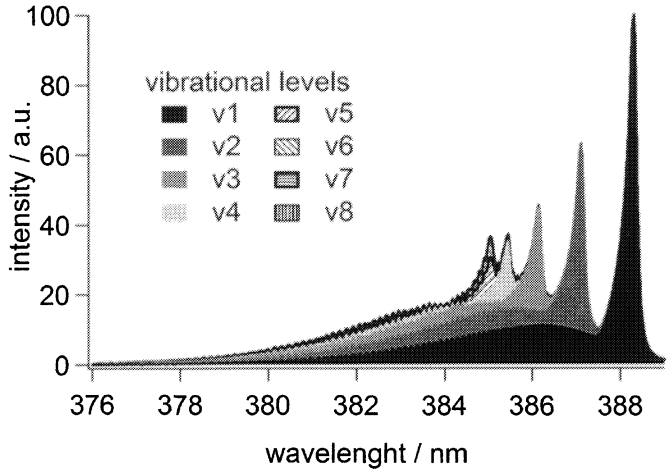

Fig. 4. Contributions of the different vibration levels to the emission of the CN-Violet system ($B^2\Sigma \rightarrow X^2\Sigma^+$).

The contributions of the different vibrational levels are shown in different gray shades and pattern. The splitting of the different rotational levels can not be distinguished as this simulation takes the resolution of our spectrometer (FWHM ≈ 1 nm) into account.

The measured spectra were then compared to the calculated spectra, and the temperature of the calculated spectra with the best correlation was assumed to be the temperature of the CN species in the plasma. The same temperature for the vibrational and rotational distribution was used to allow an automatic comparison of the calculated and measured spectra, which might be not the perfect solution in some cases.

2.2. Electron density determination

The electron density in the plasma was gained from the Stark broadening of the H-Balmer-α peak at 656 nm. The analysis of Stark-broadened spectral-line profiles is one of the most common used methods of plasma diagnosis. The physics behind this method is the broadening of the atomic emissions by the electric fields produced by nearby ions and electrons, or by the collective fields associated with plasma waves [14, 15]. The full width half maximum (FWHM) of the H-Balmer-α was measured and compared to the data published by Gigosos and Cardeneso [15], where tables list the electron densities as a function of the temperature, the ion-emitter reduced mass, and the FWHM.

2.3. Thrust measurements

To analyze the polymers for their performance in a μLPT, the target momentum was measured with a torsion balance as described in [7]. The target momentum was then used to calculate the momentum coupling coefficient C_m:

$$C_m = \frac{m\Delta v}{W} = \frac{F}{P} \text{ [dyn/W]} \quad (4)$$

where $m\Delta v$ is the target momentum produced during the ejection of laser ablated material. W is the induced laser pulse energy. F is the thrust, and P the incident power. The second important parameter for thrusters is the specific impulse I_{sp}, which is defined as:

$$I_{sp}g = v_E = C_m Q^* \text{ [cm/s]} \quad (5)$$

Q^* is the specific ablation energy (incident power/mass ablation rate), v_E is the exhaust velocity, and g is the acceleration due to gravity.

As equation 5 demonstrates, I_{sp} and C_m are not independent. If, for example, a significant amount of incident energy is absorbed as heat in the target rather then producing material ejection, Q^* will be higher and C_m well be proportionally lower. This results in the same exhaust velocity and I_{sp} for both cases .

3. RESULTS AND DISCUSSION

All polymers were investigated above the ablation threshold fluence (F_{th}) in two fluence ranges, i.e. below the plasma threshold fluence (F_{plasma}) with ns-shadowgraphy, and above F_{plasma} with emission spectroscopy.

3.1. Ablation rates

GAP reveals a similar threshold fluence for both dopants ($F_{th\ GAP+C}$ = 3100 mJ/cm^2, $F_{th\ GAP+IR}$ = 2385 mJ/cm^2), while the threshold fluence of PVC + C is significant lower, i.e. 900 mJ/cm^2. The ablation rate of PVN + C could not be obtained, as the polymer is too soft for being measured with the profilometer. The threshold fluence was therefore determined by optical microscopy ($F_{th\ PVN+C}$ =860 mJ/cm^2). The reason for the lower F_{th} for PVC + C and PVN + C is not clear.

GAP has a much higher ablation rate than PVC + C, probably due to a much higher decomposition enthalpy of GAP. The energy produced during the ablation process by the decomposition, may lead to a decomposition of additional material. Only a small difference in the ablation rate between the two dopants was found for GAP. At very high fluences (above 40 J/cm^2) a constant ablation rate is observed for GAP (not shown in Fig. 5). This effect is most probably caused by plasma shielding [16] and the breakdown of air, that also starts at this fluence.

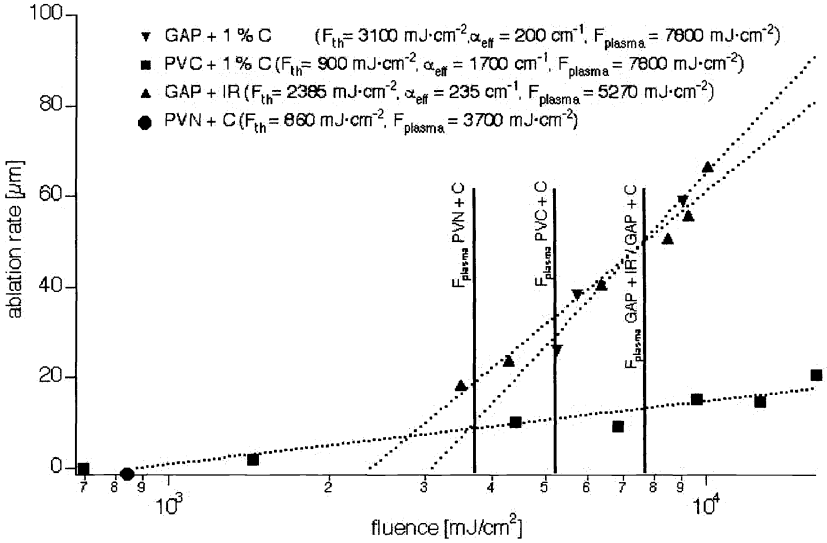

Fig. 5. Ablation rates and F_{plasma} of GAP + C, GAP + IR and PVC + C. F_{th} for PVN + C is marked as circle.

3.2. Morphology of the ablation crater

All four polymers were ablated with a single pulse at a fluence of 33 J/cm^2. The ablated spots were analyzed by optical microscopy and with a scanning electron microscope (SEM) (Fig. 6).

The energetic polymers do not redeposit a significant amount of the ejected material in the surrounding of the ablation crater. The edge of the crater is well defined, particularly in the case of GAP with both dopants. In the case of PVC + C large fragments of the polymer are redeposited in and around the ablation crater.

The carbon doped polymers reveal all a very rough crater, especially if compared to GAP doped with the IR-dye. The IR-dye is probably dispersed on a molecular level, and the light is therefore absorbed uniformly throughout the whole ablated volume, which may be the reason for the steep and smooth walls (Fig. 6. b).

Carbon nanopearls tend to agglomerate in suspensions and therefore form agglomerates of 10 to 20 µm diameter [8]. This agglomeration can result in the formation of local hotspots [17]. In the near surrounding of these particles, the material is decomposed. This decomposition leads to a formation of gaseous products and the ejection of polymer fragments between the ablation spots. The different morphologies of the ablation craters produced in PVN + C may be explained by the application of a different carbon (basic carbon sooth instead of carbon nanopearls), which may have particle sizes that are larger than the agglomerated nanopearls.

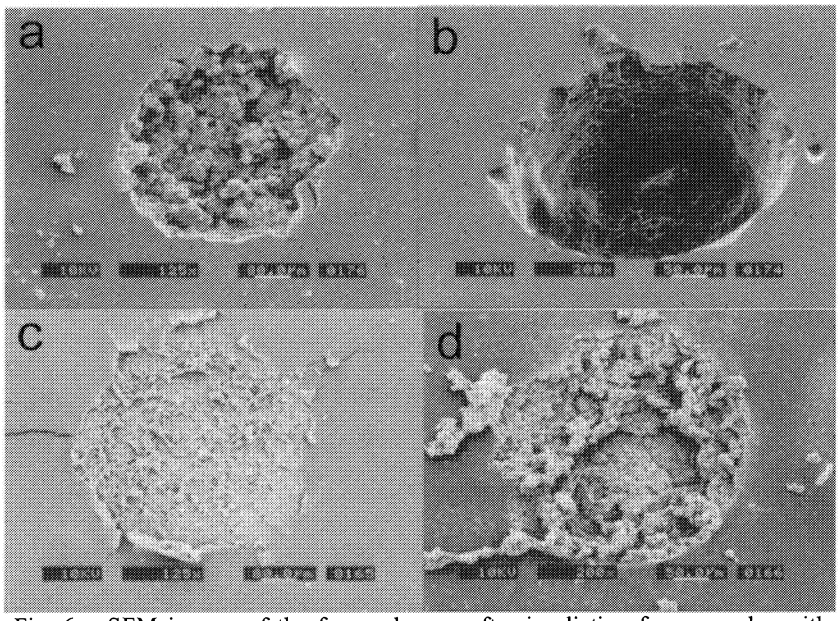

Fig. 6. SEM images of the four polymers after irradiation for one pulse with 33 J/cm^2 at 1064 nm: a) GAP + C, b) GAP + IR (image taken at an angle of 20 °), c) PVN + C, d) PVC + C

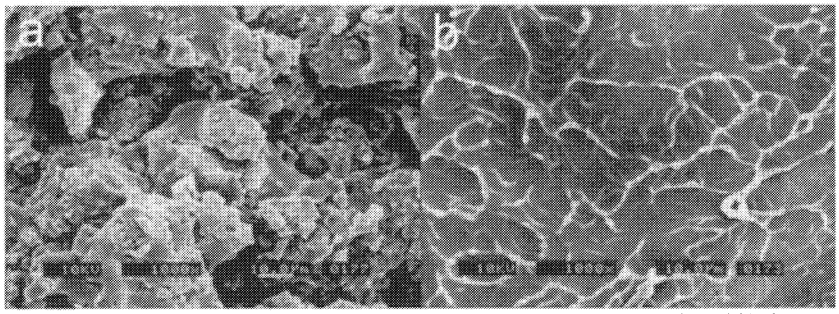

Fig. 7. SEM images of the center of the ablation spot. a) GAP + C and b) GAP + IR with 1000 times magnification.

In Fig. 7. the bottoms of the ablation craters of GAP + C and GAP + IR are shown. GAP + IR reveals a quite smooth surface with some structures that may be described as filaments. The crater of GAP + C consist of large fragments and holes in the range of 10 to 20 µm, which is in the same range as the agglomerated carbon nanoparticles.

3.3. Ns-Shadowgraphy

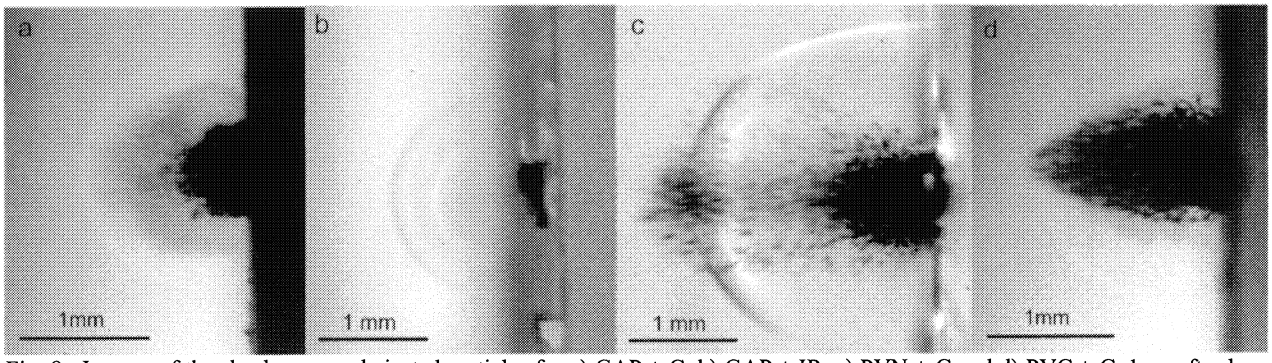

Fig. 8. Images of the shockwave and ejected particles for a) GAP + C, b) GAP + IR, c) PVN + C and d) PVC + C, 1 μs after laser irradiation.

All carbon doped polymers (Fig. 8. a), c) and d)) reveal an ejection of large polymer fragments, compared to GAP doped with IR dye, where only the shockwave is clearly visible. The shape of the shockwave for all polymers shows a similar, almost hemispherical shape, but the release of larger particles looks different for every polymer. The particles emitted from GAP + C seem to follow the expanding shockwave, whereas the particles emitted by PVC + C and PVN + C overtake the shockwave within the first microsecond. PVC + C shows a very directed expansion of the particle plume, while the PVN + C (and also of GAP + C) is separated into two parts, where the second part, consisting of large fragments, remains behind the shockwave. The first part travels faster than the shockwave and overtakes it.

The emission of larger solid and liquid fragments in carbon doped polymers, compared to GAP doped with the IR-dye can be explained by the different absorption mechanism. In the IR-dye doped GAP, the light is absorbed on a molecular level over the whole polymer layer. The material decomposes uniformly and is transferred completely into gaseous products. In the case of the carbon doped polymers, the light is absorbed by randomly distributed carbon particles and agglomerates. This leads to local hotspots, where the polymer is decomposed locally, while material between the hotspot is removed as large solid or liquid fragments by the expanding gaseous products.

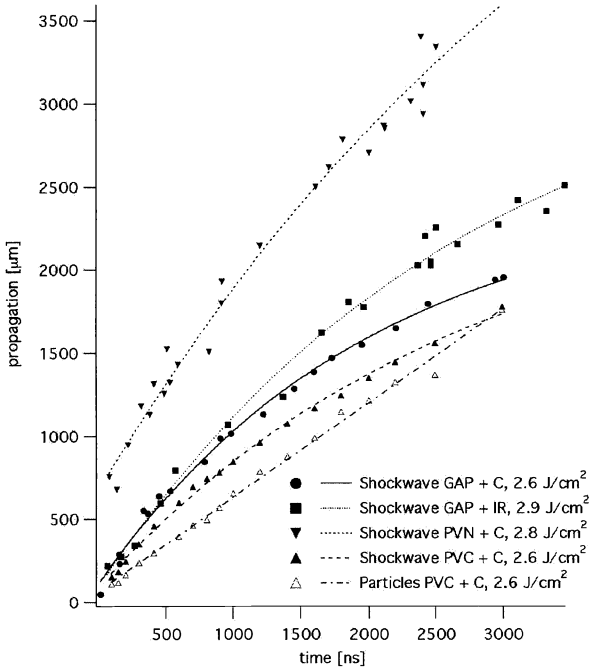

Fig.9. The propagation of the shockwave as a function of time for all polymers.

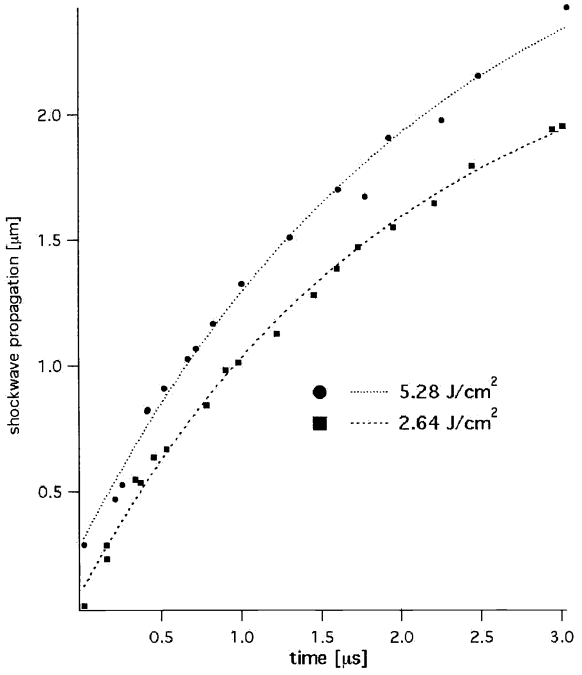

Fig. 10. The propagation of GAP + C as a function of the fluence.

The shockwave velocity is always higher for the energetic materials. PVN + C reveals the fastest shockwave velocity. The shockwave of GAP doped with the IR-dye expands slightly faster than the shockwave of the carbon doped GAP. PVC + C reveals the slowest propagation of the shockwave. For all shockwaves an exponential decrease of the velocity can be observed, which is caused by the "drag" of the air, in which the shockwaves propagates [18]. The particles ejected from PVN + C travel also much faster than those observed for GAP or PVC + C. This might be due to by the much higher decomposition enthalpy of PVN + C (-3829 J/g) compared to GAP (-2053 J/g) or PVC + C (-418 J/g)
The larger particles propagate linear as shown in Fig. 9 for PVC + C. A faster shockwave velocity for GAP + IR was expected, as more polymer is transfered into the gaseous state (no large fragments in the ablation plume), which leads to a larger production of energy.
The reduction of the shockwave velocity with less laser energy (Fig. 10) confirm this interpretation of energy into shockwave velocity.

3.4. Emission Spectroscopy

All spectra were recorded above the threshold for plasma formation (F_{plasma}). The maximum applied fluence was limited by the breakdown of air at a fluence of ≈ 40 J/cm^2.

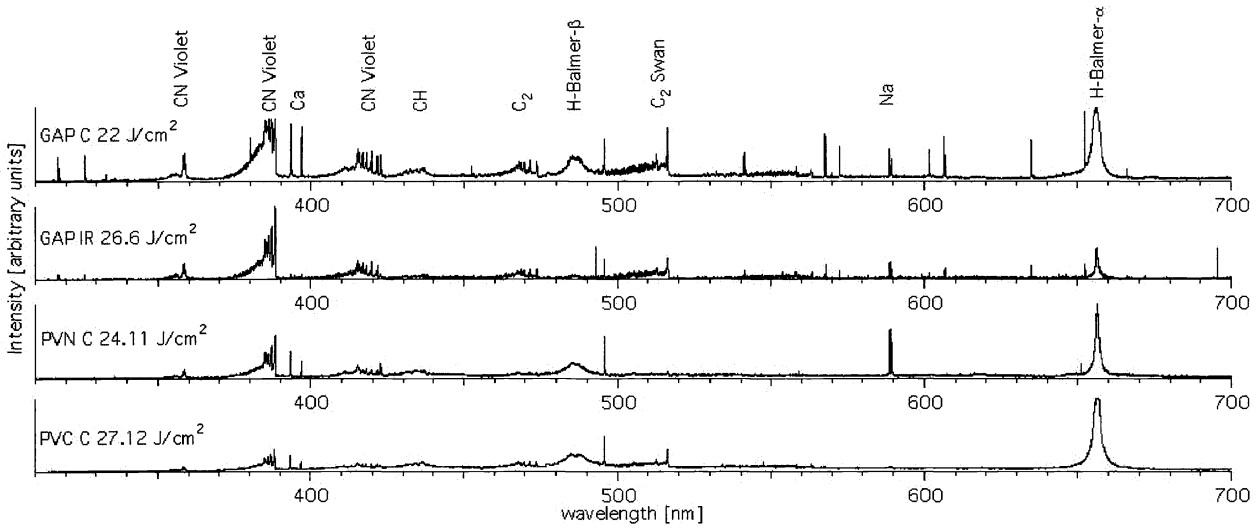

Fig. 11. Plasma emission spectra of GAP + C, GAP + IR, PVN + C and PVC + C from 300 to 700 nm recorded 1 μs after the laser pulse.

The overview spectra for all four polymers are shown for fluences between 22 and 27 J/cm^2 and a delay time of one μs after irradiation (in Fig. 11).

All spectra for the carbon doped polymers reveal the presence of diatomic (CN Violet, C_2 and CH) [19] and atomic (H, Ca and Na) species. The hydrogen is most probably created during the fragmentation of the polymer, while Ca seems to be a common impurity in carbon. Ca lines are observed in all three spectra of carbon doped polymer, whereas they are not visible in the polymer doped with the IR-dye.
The peaks of the IR-dye doped GAP are generally less intense compared to the carbon doped GAP. Only the CN Violet and the C_2 Swan systems are clearly visible, while from the atomic peaks only H-Balmer-α at 656 nm can be observed. The H-Balmer-β peak at 486 nm can only barely be distinguished from the background.
The CN Violet system in the PVC + C spectra must be created by reaction of the excited C species emitted from the polymer with N_2 from the surrounding air, to form CN [20].

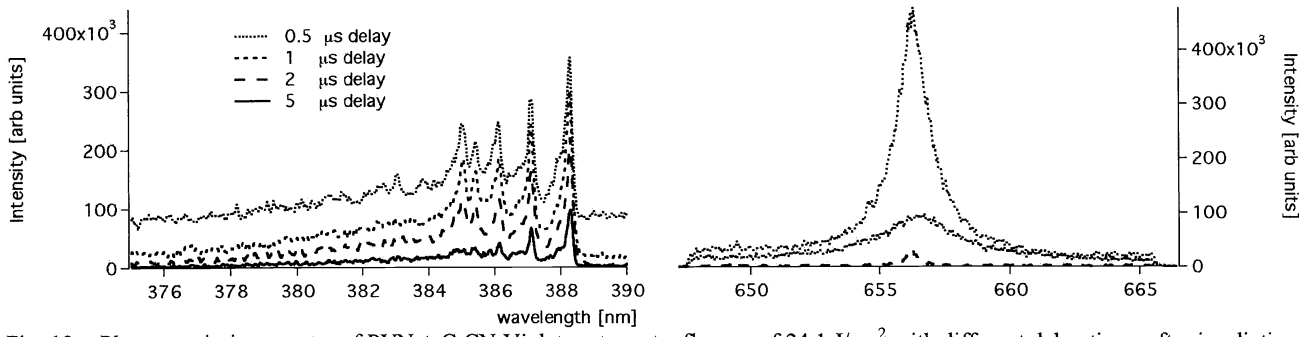

Fig. 12. Plasma emission spectra of PVN + C CN Violet system at a fluence of 24.1 J/cm^2 with different delay times after irradiation. The CN Violet system at 389 nm is shown on the left, while H-Balmer-α at 656 nm is shown on the right.

The intensity of the atomic peaks decreases much faster with time as the molecular peaks, as shown in Fig. 12. The H-Balmer-α has almost dissapeared after 2 µs, whereas the CN Violet system can be observed until 10 to 20 µs after the creation of the plasma (for similar starting intensities).

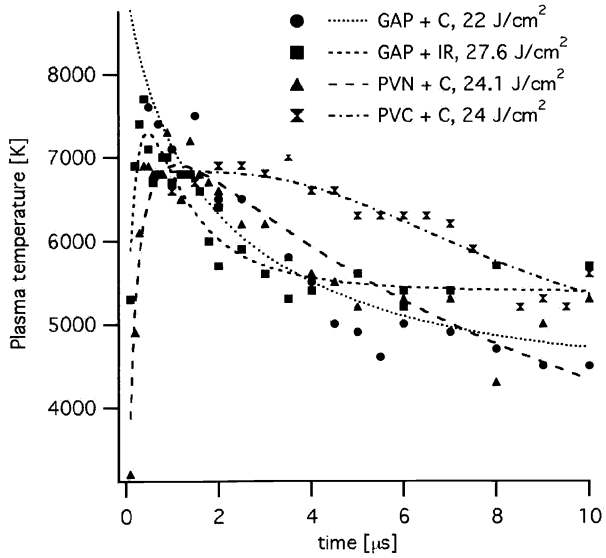

Fig. 13.Plasma temperature versustimefor all polymers.

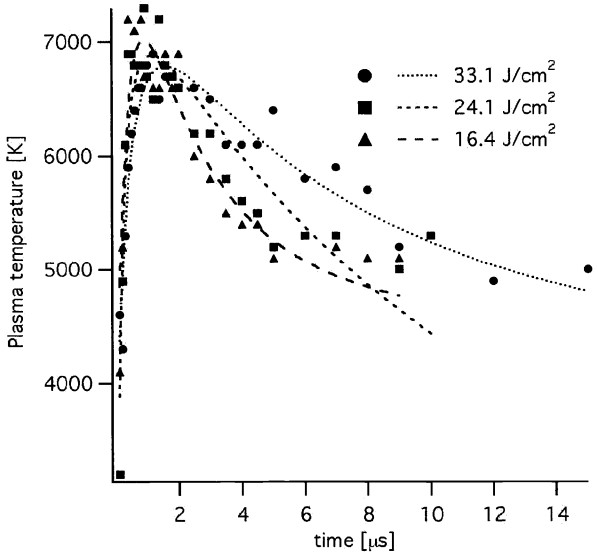

Fig. 14. The influence of different fluences on the plasma temperature for of PVN + C.

The change of the plasma temperature with the delay time is shown in Fig. 13. The plasma temperatures were calculated by the simulation of the ro-vibrational spectra of the CN violet system at 389 nm as described in section 2.1.
The energetic polymers reveal a higher maximum temperature compared to PVC + C, but the decay is much faster than the almost linear decay of PVC + C. No pronounced influence of the IR-dye on the plasma temperature could be detected. The influence of the fluence on the plasma temperature is displayed in Fig. 14 for PVN + C. Higher fluences result in a lower maximum temperature, but also a slower decay with time.

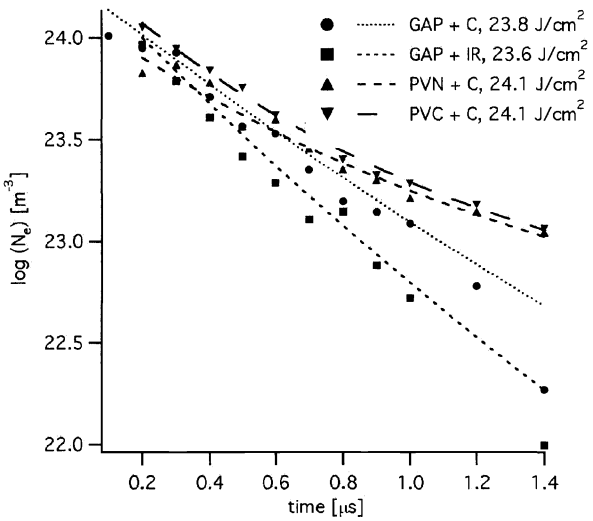

Fig. 15. The decrease of the electron density for all polymers.

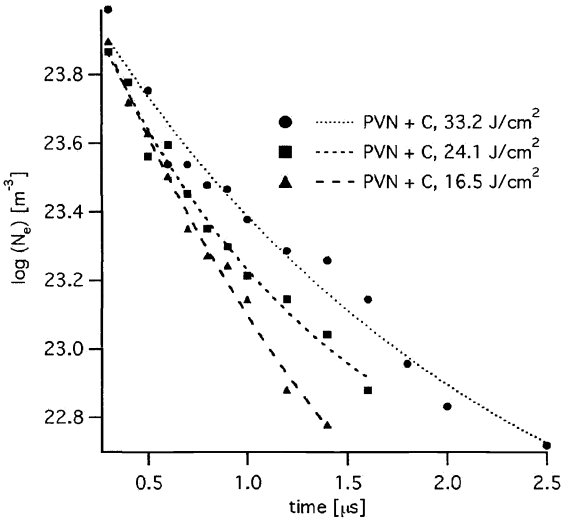

Fig. 16. The influence of different fluences on the electron density in the case of PVN + C.

The initial electron density in the plasma determined from the H-Balmer-α peak is similar for all polymers (Fig. 15). GAP shows a steeper decrease with both dopants than PVN + C and PVC + C. Increasing the fluences does not change the initial value, but changes the decay rate as shown in Fig. 16

The decrease in the electron density takes place in the same time scale as the plasma temperature increases, which could be caused by an energy transfer from the free electrons to the CN system (Fig. 17).

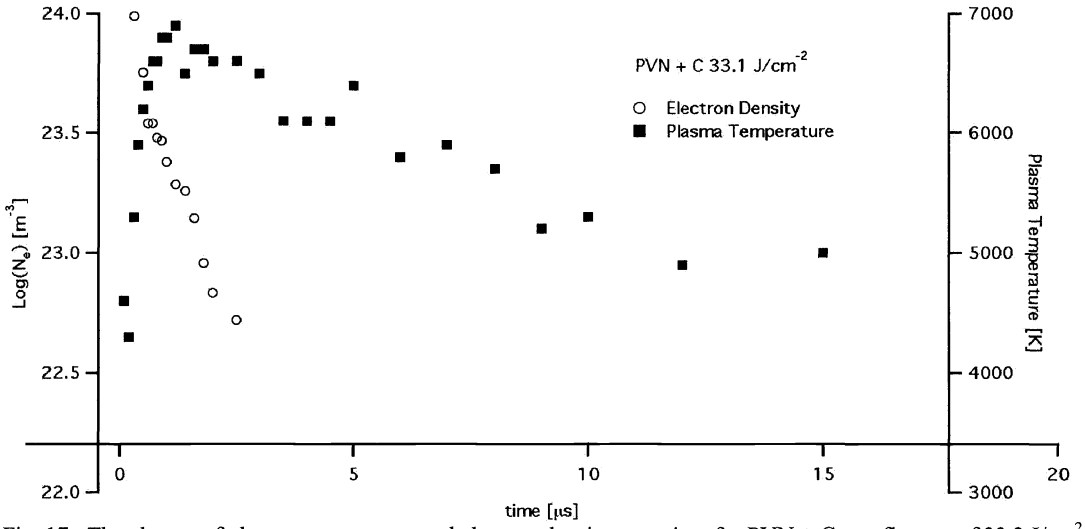

Fig. 17. The change of plasma temperature and electron density over time for PVN + C at a fluence of 33.2 J/cm^2.

3.5. Thrust, momentum coupling and specific impulse

GAP + C shows a well defined threshold for an increase of C_m, as shown in Fig. 18. This is an important feature for the design of a μLPT with a tape-like polymer fuel, because the optimum incident laser fluence and tape speed are clearly defined [1]. This increase in C_m at the threshold can also be seen for PVC + C (Fig. 19), but it is not as well defined as for GAP + C.

In Fig. 18, values for C_m of up to 50 dyn/W (500 μN/W) and maximum I_{sp} of 550s were obtained for GAP + C, which result in a maximum product of C_m x I_{sp} = 16,870. This is equivalent to 83% of the theoretical maximum for a perfectly efficient non-energetic absorber and also implies an exhaust velocity of 5.4 km/s. Other experiments have also shown

that the theoretical maximum of 100% can be exceeded, which shows that the decomposition enthalpy of the polymer can also be utilized for creating thrust.
PVC + C reveals a nearly constant C_m value of 6.2 dyn/W (62 μN/W) above the threshold and a specific impulse I_{sp} of even larger than 1000 s (Fig. 19).

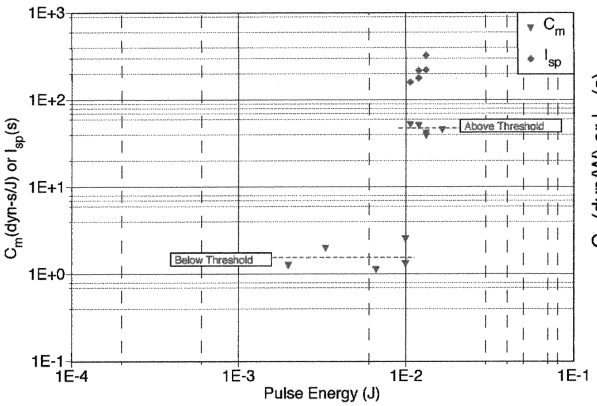

Fig. 18. Coupling coefficient and specific impulse measurec with single pulses from the single-mode research laser focused to 5μm spot diameter on GAP + C

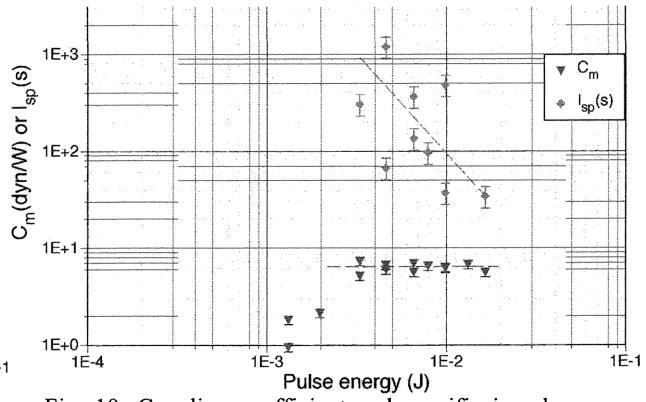

Fig. 19. Coupling coefficient and specific impulse measured with single pulses from the single-mode research laser focused to 5μm spot diameter, on standard PVC/Acetate target material in T mode

GAP + C (1170 μN/W) shows a higher maximum C_m than both PVN + C (120 μN/W) and PVC + C (83 μN/W) (Fig. 20). The specific impulse is only slightly lower for GAP + C than for PVC + C. The lowest values for both C_m and I_{sp} are found for PVN + C, although it has the highest decomposition enthalpy. The reason for this low performance is not yet clear, but may be caused by a non optimized polymer dopant system.

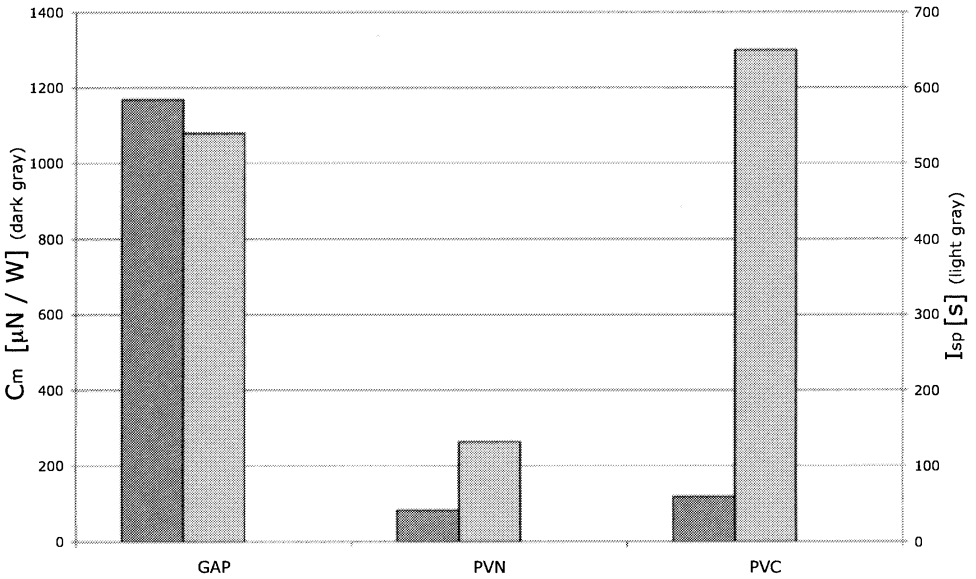

Fig. 20. Comparison of the maximum C_m and I_{sp} for GAP + C, PVN + C and PVC + C obtained in the impulse test stand.

GAP + C reveals the best thrust data of all investigated polymers, while measurements for GAP + IR were not yet performed, but a similar behavior to GAP + C could be expected, as for all other measurements above F_{plasma} similar results were obtained.

4. CONCLUSIONS

The different dopants for GAP seem to have only little influence in the ablation properties, such as F_{th} and F_{plasma}. The most pronounced differences are observed in the fragments ejection detected in the shadowgraphy measurements and the crater appearance. Large fragments of solid and liquid ablation products are observed for GAP + C, while almost no solid fragments are ejected by GAP + IR. It seems, that the ablated material is transferred completely into gaseous products. The SEM images confirm these results, by showing that an ablation crater with steep, smooth walls is obtained for GAP + IR, whereas the crater of GAP + C is quite rough, with deep holes and a very uneven bottom. This difference can be explained by the different distribution of the dopant in the polymer. The IR-dye should be distributed on a molecular level, whereas carbon tends to agglomerate and to form particles of 10 to 20 μm in size.

For all carbon doped polymers, the ablation spots have a similar morphology. A very rough crater with some redeposited ablation products was observed. The shadowgraphy measurements of PVN + C reveal, that the shockwave and particle plume propagates faster than in the case of the other polymers. The particle plumes showed a very different expansion behavior for all polymers. In the case of GAP + C an almost hemispherical expansion was observed. The particle plume of PVN + C and PVC + C were more directional (perpendicular to the surface). The large particles overtake the shockwave within the first μs.

The plasma temperature and electron density measurements showed no significant difference for all energetic polymers. Only PVC + C displayed a slower almost liner decay of the plasma temperature over time. An increase of the plasma temperature could be observed during the first micro second.
The electron density for GAP decreased slightly faster than for PVN + C and PVC + C. For all polymers the decrease of the electron density takes place in the same time scale, where the plasma temperature increases, i.e. within 1 μs.

The thrust measurements showed the best results for GAP + C. PVN + C displays rather poor thrust properties, in spite of the highest decomposition enthalpy. The shadowgraphy measurements of PVN + C revealed a fast propagation of the shockwave, the low thrust values for PVN + C are comparable to data acquired for PVC + C.

ACKNOWLEDGEMENTS

The authors would like to thank M. Nagel (EMPA, Dübendorf, Switzerland) and Nitro Chemie Wimmis for supplying some of the materials. This work is supported by the European Office of Aerospace Research and Development (London) under contract FA865-03-1-3058 (Project 042076) and the Swiss National Science Foundation.

REFERENCES

1. C. Phipps, J. Luke, T. Lippert, "Laser ablation of organic coatings as a basis for micropropulsion", *Thin Solid Films*, **453-454**, 573-583, 2004
2. C.R. Phipps, J.R. Luke, G.G. McDuff, T. Lippert, "Laser-driven micro-rocket", *Appl. Phys. A-Mater. Sci. Process.*, **77**, 193-201, 2003
3. T. Lippert, C. David, M. Hauer, T. Masubuchi, H. Masuhara, K. Nomura, O. Nuyken, C. Phipps, J. Robert, T. Tada, K. Tomita, A. Wokaun, "Novel applications for laser ablation of photopolymers", *Appl. Surf. Sci.*, **186**, 14-23, 2002
4. T. Lippert, M. Hauer, C.R. Phipps, A. Wokaun, "Fundamentals and applications of polymers designed for laser ablation", *Appl. Phys. A-Mater. Sci. Process.*, **77**, 259-264, 2003
5. C. Phipps, J. Luke, G.G. McDuff, T. Lippert, eds. *Laser Ablation Powered Mini-Thrusters.* High-Power Laser Ablation IV, Proceedings of the SPIE, ed. C. Phipps. Vol. 4760. 2002, SPIE.
6. D.S. Moore, S.D. McGrane, "Comparative infrared and Raman spectroscopy of energetic polymers", *J. Mol. Struct.*, **661**, 561-566, 2003
7. C. Phipps, J. Luke, "Diode laser-driven microthrusters: A new departure for micropropulsion", *Aiaa J.*, **40**, 310-318, 2002
8. R.P. Richner,DISS. ETH Nr. 14413, *Entwicklung neuartig gebundener Kohlenstoffmaterialien für elektrische Doppelschichtkondensatorelektroden.* 2001, ETH, Zürich

9. R. Srinivasan, B. Braren, "Ablative Photodecomposition of Polymer-Films by Pulsed Far- Ultraviolet (193 Nm) Laser-Radiation - Dependence of Etch Depth on Experimental Conditions", *J. Polym. Sci. Pol. Chem.*, **22**, 2601-2609, 1984
10. J.E. Andrew, P.E. Dyer, D. Forster, P.H. Key, "Direct Etching of Polymeric Materials Using a Xecl Laser", *Appl. Phys. Lett.*, **43**, 717-719, 1983
11. J. Luque, D.R. Crosley, *LIFBASE: Database and Spectral Simulation Program (version 1.6)*. 1999, SRI International Report MP 99-099.
12. I. Kovacs, *Rotational structure in the spectra of diatomic molecules*, Adam Hilger Ltd., London, 1969
13. L.T. Earls, *Phys. Rev.*, **48**, 423, 1935
14. H.R. Griem, *Principles of Plasma Spectroscopy*, Cambridge University Press, Cambridge, 1997
15. M.A. Gigosos, V. Cardenoso, "New plasma diagnosis tables of hydrogen Stark broadening including ion dynamics", *J. Phys. B-At. Mol. Opt. Phys.*, **29**, 4795-4838, 1996
16. R.K. Singh, "Transient plasma shielding effects during pulsed laser ablation of materials", *J. Electron. Mater.*, **25**, 125-129, 1996
17. X.N. Wen, D.E. Hare, D.D. Dlott, "Laser Polymer Ablation Threshold Lowered by Nanometer Hot-Spots", *Appl. Phys. Lett.*, **64**, 184-186, 1994
18. J. Gonzalo, C.N. Afonso, I. Madariaga, "Expansion dynamics of the plasma produced by laser ablation of BaTiO3 in a gas environment", *J Appl Phys*, **81**, 951-955, 1997
19. G. Herzberg, *Spectra of Diatomic Molecules*, D. Van Nostran Company, INC., New York, 1950
20. S.S. Harilal, R.C. Issac, C.V. Bindhu, P. Gopinath, V.P.N. Nampoori, C.P.G. Vallabhan, "Time resolved study of CN band emission from plasma generated by laser irradiation of graphite", *Spectrochim Acta A*, **53**, 1527-1536, 1997